







Assembly and organization of the N-terminal region of mucin MUC5AC: Indications for structural and functional distinction from MUC5B

Jerome Carpenter^{a,b,1} , Yang Wang^{a,b,1}, Richa Gupta^{a,b,1} , Yuanli Li^{a,b}, Prashamsha Haridass^{a,b}, Durai B. Subramani^a, Boris Reidel^{a,b}, Lisa Morton^a, Caroline Ridley^{c,d}, Wanda K. O'Neal^a, Marie-Pierre Buisine^e , Camille Ehre^a, David J. Thornton^{c,d} , and Mehmet Kesimer^{a,b,2}

^aMarsico Lung Institute, University of North Carolina at Chapel Hill, Chapel Hill, NC 27517-7248; ^bDepartment of Pathology and Laboratory Medicine, University of North Carolina at Chapel Hill, Chapel Hill, NC 27517-7248; ^cWellcome Trust Centre for Cell-Matrix Research, Faculty of Biology, Medicine and Health, The University of Manchester, Manchester M13 9PL, United Kingdom; ^dThe Lydia Becker Institute of Immunology and Inflammation, Faculty of Biology, Medicine and Health, The University of Manchester, Manchester M13 9PL, United Kingdom; and ^eUMR9020-U1277 CANTHER (Cancer Heterogeneity Plasticity and Resistance to Therapies), Université Lille, CNRS, Inserm, CHU Lille, F5900 Lille, France

Edited by Scott J. Hultgren, Washington University School of Medicine, St. Louis, MO, and approved August 23, 2021 (received for review March 8, 2021)

Elevated levels of MUC5AC, one of the major gel-forming mucins in the lungs, are closely associated with chronic obstructive lung diseases such as chronic bronchitis and asthma. It is not known, however, how the structure and/or gel-making properties of MUC5AC contribute to innate lung defense in health and drive the formation of stagnant mucus in disease. To understand this, here we studied the biophysical properties and macromolecular assembly of MUC5AC compared to MUC5B. To study each native mucin, we used Calu3 monomucin cultures that produced MUC5AC or MUC5B. To understand the macromolecular assembly of MUC5AC through N-terminal oligomerization, we expressed a recombinant whole N-terminal domain (5ACNT). Scanning electron microscopy and atomic force microscopy imaging indicated that the two mucins formed distinct networks on epithelial and experimental surfaces; MUC5B formed linear, infrequently branched multimers, whereas MUC5AC formed tightly organized networks with a high degree of branching. Quartz crystal microbalance-dissipation monitoring experiments indicated that MUC5AC bound significantly more to hydrophobic surfaces and was stiffer and more viscoelastic as compared to MUC5B. Light scattering analysis determined that 5ACNT primarily forms disulfide-linked covalent dimers and higher-order oligomers (i.e., trimers and tetramers). Selective proteolytic digestion of the central glycosylated region of the full-length molecule confirmed that MUC5AC forms dimers and higher-order oligomers through its N terminus. Collectively, the distinct N-terminal organization of MUC5AC may explain the more adhesive and unique viscoelastic properties of branched, highly networked MUC5AC gels. These properties may generate insight into why/how MUC5AC forms a static, “tethered” mucus layer in chronic muco-obstructive lung diseases.

mucin | MUC5AC | lung | mucus gel | airways

Gel-forming mucins are an essential component of the mucus layer that covers and protects epithelial surfaces from environmental insults. The mucin composition of mucus lining different mucosal surfaces depends on the functional requirements imposed on the epithelium. For instance, in the small intestine and colon, which harbor diverse microbiota, MUC2 is the mucin structurally adapted to form a “tight mucus layer” that provides a niche for the microbes and protects the underlying epithelia by preventing bacterial invasion (1). While in the stomach, MUC6 and MUC5AC together provide a barrier that protects the epithelium from the harsh effects of high luminal acidity (pH = 2 to 3) (2). The mouth, which is the major portal of food and microbes, is protected by saliva, and the dominant gel-forming mucin is MUC5B (3). The lungs, another major portal with exposure to the environment, are mainly protected during homeostasis by MUC5B with a lesser contribution by MUC5AC (4, 5). The distinct regions of the airways have different functional and innate

protective requirements for homeostasis, and this necessitates the diverse expression patterns of both mucins throughout the respiratory system (6). MUC5B, secreted by cells in the submucosal glands and the surface epithelium (6), has been shown to be essential for lung innate defense (7). MUC5AC, secreted only by cells in the surface epithelium mainly in the larger airways (6), is generally produced in response to stresses such as cigarette smoke and allergens and is closely associated with muco-obstructive lung diseases, including chronic bronchitis (CB), chronic obstructive pulmonary disease (COPD) (4, 8), and asthma (9, 10). MUC5AC is also critical for defense against enteric parasites, some of which invade the lung (11).

Both MUC5B and MUC5AC are large (2 to 100 MDa), polymeric glycoproteins with a high degree of sequence similarity and domain homology, particularly in their N- and carboxyl-terminal regions (12–15). Similar to MUC5B, the N-terminal region of MUC5AC contains von Willebrand factor-like domains (D1, D2, and D3) in addition to trypsin inhibitory-like (TIL) domains and

Significance

Gel-forming mucins, MUC5AC and MUC5B, are the essential components of the protective mucus layer of the lungs. MUC5B is crucial for lung innate defense, and MUC5AC is generally secreted disproportionately in response to cigarette smoke and allergens. MUC5AC's role in airway defense and chronic airway disease pathogenesis and how this emerges from its macromolecular assembly/gel-making properties are not known. We demonstrate MUC5AC binds significantly more to hydrophobic surfaces and forms stiffer and more viscoelastic layers compared to MUC5B. Also, MUC5AC forms higher-order oligomers in addition to dimers. These observations may generate insight into why/how MUC5AC forms a stagnant, “tethered” mucus layer in muco-obstructive lung diseases and could guide the development of strategies to intervene with more effective therapeutic agents.

Author contributions: Y.W., R.G., W.K.O., D.J.T., and M.K. designed research; J.C., Y.W., R.G., Y.L., P.H., B.R., L.M., C.R., C.E., and M.K. performed research; J.C., Y.W., R.G., D.B.S., and M.-P.B. contributed new reagents/analytic tools; J.C., B.R., and M.K. analyzed data; and J.C., Y.W., D.J.T., and M.K. wrote the paper.

The authors declare no competing interest.

This article is a PNAS Direct Submission.

Published under the PNAS license.

¹J.C., Y.W., and R.G. contributed equally to this work.

²To whom correspondence may be addressed. Email: kesimer@med.unc.edu.

This article contains supporting information online at <https://www.pnas.org/lookup/suppl/doi:10.1073/pnas.2104490118/-DCSupplemental>.

Published September 21, 2021.

unique regions. The N terminus is followed by a central, highly *O*-glycosylated mucin domain, which is interrupted by cysteine-rich (CysD) domains and a carboxyl-terminal region that mediates dimerization. In contrast to other gel-forming mucins, MUC5AC contains a putative leucine zipper (LZ) domain (16) at the end of the carboxyl-terminal end of the D1 domain of the N terminus, with no known function.

The major gel-forming mucins (MUC2, MUC5AC, MUC5B, and MUC6) assemble intracellularly to form polymers, first via disulfide-linked dimerization between their carboxyl termini and then via disulfide-linked N-terminal multimerization. However, knowledge of multimerization is incomplete. The MUC5B N-terminal region is assembled exclusively as dimers (17). However, assembly of the MUC2 N-terminal region is more controversial, and it has been reported to assemble solely as trimers (18) or dimers (19). The N-terminal assembly of MUC5AC has not been investigated. It is thought that the unique structural organization of the different gel-forming mucins results in mucus gels optimized to meet the functional demands and provide proper protection to the diverse epithelial environments across the body.

MUC5AC mucin production is modulated by both type 1 [e.g., in response to viral infections (20, 21) and cigarette smoke (22)] and type 2 [e.g., in response to allergens (9)] immune responses, associated with lung disease and, indeed, disproportionately increases as compared to MUC5B (4, 8, 9, 23, 24). How MUC5AC contributes to both innate defense of the lung and the pathogenesis of chronic obstructive lung diseases remains unclear. As a first step of understanding the structural, organizational, and functionally distinctive properties of MUC5AC mucin and how these properties may affect the mucus gel organization/properties as compared to the other major lung mucin, MUC5B, we investigated the nature of MUC5AC multimeric organization through its N-terminal domain using an expressed recombinant protein (5ACNT), with a focus on the unique LZ region at the carboxyl-terminal end of the D1 domain. To understand if the LZ region has an organizational role in the assembly of the N-terminal region of MUC5AC, we mutated the four leucine residues in the LZ region of 5ACNT.

Results

Supramolecular Structure of the Mucus Gels Formed by MUC5AC and MUC5B from Calu3 Monomucin Cultures. MUC5AC and MUC5B monomucin Calu3 cultures (CRISPR-Cas9 manipulated to produce either only MUC5AC or MUC5B), as well as wild-type (WT) Calu3 cells (produce both MUC5AC and MUC5B, typically at a 3:1 ratio), were subjected to scanning electron microscopy (SEM) analysis using a Zeiss Supra 25 field emission SEM at 5 kV. Imaging revealed distinct structures of MUC5AC and MUC5B mucin gels produced by the monomucin Calu3 cultures, while mucin gels from WT Calu3 cells exhibited features of both (Fig. 1). The SEM images indicate that the mucins form distinct mucus network structures; MUC5AC exhibits a much tighter infrastructure, with branched/cross-linked mucins and little evidence of linear thread formation. In contrast, MUC5B gel structure is dominated by linear, less-branched, hair-like mucin strands/bundles (Fig. 1). The SEM images of the mucin gels from WT Calu3 cultures showed a combination of both branched/cross-linked and linear threads and demonstrate the features typical of an airway mucus gel network (Fig. 1 *E* and *F*).

Macromolecular Organization of MUC5AC and MUC5B Mucins in Concentrated and Dilute Conditions. To further characterize the macromolecular organization and the network characteristics of individually isolated MUC5AC and MUC5B mucins (from monomucin Calu3 cultures), and a combination of both (from native Calu3 cells), atomic force microscope (AFM) imaging was used. In general, as observed with the SEM images of MUC5AC and MUC5B mucus layers in Fig. 1, the MUC5AC network tended to

form tightly organized multimers with a high degree of branching in concentrated and dilute conditions (Fig. 2 *A* and *D*). In contrast, the MUC5B network again featured long linear polymers with little branching (Fig. 2 *B* and *E*). The network of a native mixture of MUC5AC and MUC5B from WT Calu3 cultures revealed a combination of long linear filaments and branched, more cross-linked structures (Fig. 2 *C* and *F*). Similar network structures were observed when purified MUC5AC and MUC5B mixed together 1:1 (*SI Appendix*, Fig. S1).

Further AFM analyses of more dilute preparations indicated that MUC5AC macromolecules have a low aspect ratio ($2.0 \pm \text{SD } 0.9$), while MUC5B macromolecules have a much higher aspect ratio ($6.1 \pm \text{SD } 4.4$) (Fig. 3*C*). To further characterize the macromolecular properties of MUC5AC and MUC5B, size-exclusion chromatography multiangle laser light scattering (SEC-MALLS) analyses of the individually purified mucins isolated from their respective monomucin Calu3 cultures were performed. Differences in MUC5AC and MUC5B polymer organization were also apparent in solution. The molecular weight (MW) and the radius of gyration (Rg) of MUC5B were ~ 25 MDa and 224 nm, respectively, whereas MUC5AC had a MW of ~ 17 MDa and an Rg of 187 nm (Fig. 3 *D* and *E*).

Assessing the Interactions of MUC5AC and MUC5B with Hydrophobic Surfaces. To numerically evaluate the biophysical properties of individual mucin preparations, quartz crystal microbalance with dissipation monitoring (QCM-D) was used. Binding of MUC5AC or MUC5B to gold-coated QCM-D chips was monitored by measuring the frequency and the dissipation shifts of multiple overtones. Experiments were performed with mucin solutions at the same mass concentration; however, the final layer properties are independent of concentration, provided that there is enough material to form a complete layer with stable signals (*SI Appendix*, Fig. S2). Using a 100- $\mu\text{g}/\text{mL}$ mucin solution, it typically took about 20 to 30 min to form a steady-state layer. The steady-state MUC5AC layer had a frequency shift of -65 Hz from the baseline in $\Delta F_{3/3}$, while the ΔD_3 dissipation increased to ~ 10 $1\text{E}-6$ (Fig. 4*A*). For the MUC5B layer, the $\Delta F_{3/3}$ frequency shifted by -40 Hz, while the ΔD_3 dissipation increased to ~ 11 $1\text{E}-6$ (Fig. 4*A*). Plotting the change in dissipation (ΔD) versus the change in frequency (ΔF) provides an overall picture of the viscoelastic properties of the resulting layers. In such a plot, the slope, $\Delta D/\Delta F$, is inversely related to the stiffness and density of the material layer (i.e., a stiffer/denser layer would have a smaller slope as compared to a sparser, “fluffier/softer” layer). Plotting $\Delta D_3/\Delta F_3$ for each mucin showed that MUC5AC had a smaller slope as compared to MUC5B, which indicates that MUC5AC forms a stiffer, denser layer. Albumin, which is known to form a rigid layer, has its $\Delta D_3/\Delta F_3$ profile plotted on the same axes for comparison and has a smaller slope than either of the mucins (Fig. 4 *B* and *C*). Using the Sauerbrey model (25), the quantity of the MUC5AC and MUC5B bound to the surface was calculated to be $964 \pm \text{SD } 159$ $\text{ng} \cdot \text{cm}^{-2}$ and $526 \pm \text{SD } 39$ $\text{ng} \cdot \text{cm}^{-2}$ ($P = 0.0018$, $n = 4$), respectively (Fig. 4*D*). Moreover, the MUC5AC layer was much thinner/denser (32.6 $\text{nm} \pm 4.4$, $n = 4$) compared to the MUC5B layer (77.4 $\text{nm} \pm \text{SD } 19.7$, $n = 4$; $P = 0.0045$) (Fig. 4*E*). Voight modeling (26) with the Q-tools software package determined that the relative viscosity (1.105 centipoise (cP) $\pm \text{SD } 0.06$, $n = 4$, $P = 0.02$) and shear elasticity (10.6 $\text{kPa} \pm \text{SD } 3.8$ $n = 4$) of MUC5AC layers were significantly higher compared to MUC5B layers, relative viscosity (0.87 $\text{cP} \pm \text{SD } 0.01$, $n = 4$), and shear elasticity (3.3 kilopascal $\pm \text{SEM } 1.4$, $n = 3$) ($P = 0.02$) (Fig. 4 *F* and *G*).

Characterization of MUC5AC N-Terminal Multimers: Western Blot and SEC-MALLS Analysis of 5ACNT Protein. To elucidate the molecular organization and structure of the MUC5AC N-terminal region, the entire N-terminal region of MUC5AC (5ACNT, theoretical MW = 141,201), containing all of the native domains (including D1-D2-D'-D3, LZ, and TIL domains) was expressed (Fig. 5*A*).

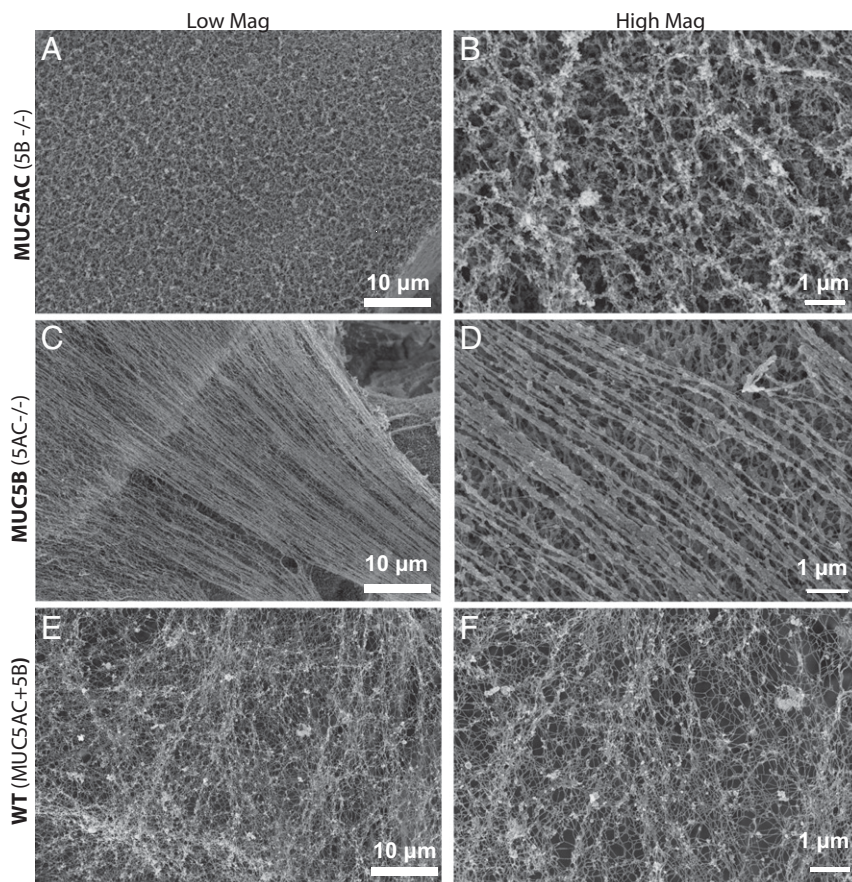


Fig. 1. SEM images of the apical surfaces of Calu3 monomucin cultures indicate that MUC5AC and MUC5B create distinct supramolecular frameworks: Calu3 cultures were grown on 12-well transwells for 10 d and subjected to SEM analysis on a Zeiss Supra 25 field emission SEM at 5 kV. The MUC5AC monomucin culture (A and B) shows a mucus gel that is tighter, more branched/cross-linked, and has no indication of linear threads/bundles formation, while the MUC5B monomucin culture mucus gel (C and D) is dominated by linear, less-branched, hair-like mucin strands. E and F show the surfaces of WT Calu3 cells, which produce both MUC5AC and MUC5B and have structural elements of both gels produced by monomucin cultures.

The expressed 5ACNT protein product was isolated from ~5 L conditioned 293-EBNA (Epstein-Barr nuclear antigen) cell line media by nickel affinity column chromatography followed by a combination of SEC and anion exchange chromatography. The final product was analyzed by sodium dodecyl sulfate–polyacrylamide gel electrophoresis (SDS-PAGE) in both native and reduced states (Fig. 5B). The SDS-PAGE profile indicated that 5ACNT was expressed dominantly as dimers and higher-order oligomers as well as a less intense monomer band (Fig. 5B). After reduction with dithiothreitol (DTT), a dominant protein band appeared around 140 kDa in size (Fig. 5B). We used the combination of Size-Exclusion Chromatography with Multi Angle Laser Light Scattering and differential Refractive Index (SEC-MALLS-dRI) to further determine the MW of the products and measured different species across the MW distribution with masses of 142.9 kDa (\pm 4.1%), 281.6 kDa (\pm 1.4%), 426.3 kDa (\pm 1.5%), and 538.6 kDa (\pm 2.5%), which correspond to a monomer, dimer, trimer, and a likely tetramer, respectively (Fig. 5C and D). To test whether these multimers were noncovalently linked, we included higher SDS percentages (5%) in addition to a chaotropic agent (6 M urea) added to the sample buffer for SDS-PAGE analysis. The results indicated that the presence of high SDS percentages and urea did not affect the band patterns observed (SI Appendix, Fig. S3).

Calcium-mediated interactions of the N-terminal region of MUC5B at low pH have been shown to be important for facilitating compact packaging in secretory granulates (17). To investigate the effect of Ca^{2+} and low pH on the multimeric organization

of 5ACNT, the protein was equilibrated overnight with buffers containing either 10 mM Ca^{2+} or 10 mM ethylenediaminetetraacetic acid (EDTA) (performed at both pH 6.0 and pH 7.4). The SEC-MALLS analyses indicated no significant effect of Ca^{2+} and pH 6.0 as compared to EDTA and pH 7.4 on the macromolecular organization of 5ACNT (SI Appendix, Fig. S4).

StcE Digestion of Full-Length MUC5AC Reveals that the MUC5AC N Terminus Assembles via Disulfide-Linked Dimers and Higher-Order Multimers. To test whether native MUC5AC exhibits similar N-terminal multimerization to that observed for the 5ACNT recombinant protein, native MUC5AC mucin was incubated with StcE, an enzyme that cleaves within *O*-linked glycosylation domains and leaves the non-*O*-glycosylated regions, including the N- and carboxyl-terminal regions, intact (27). Notably, StcE is not predicted to disrupt disulfide bonds between the multimerized N termini. After StcE digestion, SDS-PAGE and Western blot analysis with antibodies specific to the N-terminal D2 and D3 domains of MUC5AC indicated D2/D3 antibody reactive bands at ~350 kDa and ~520 kDa in unreduced preparations (Fig. 5E). In the reduced preparations, a single band around 170 kDa was observed (Fig. 5E). No D2/D3 antibody reactivity was observed in the resolving gel for nontreated unreduced preparations, but after reduction, a large band was visible at the origin of the gel, representing undigested monomers of MUC5AC (approximate MW of 2 to 2.5 MDa).

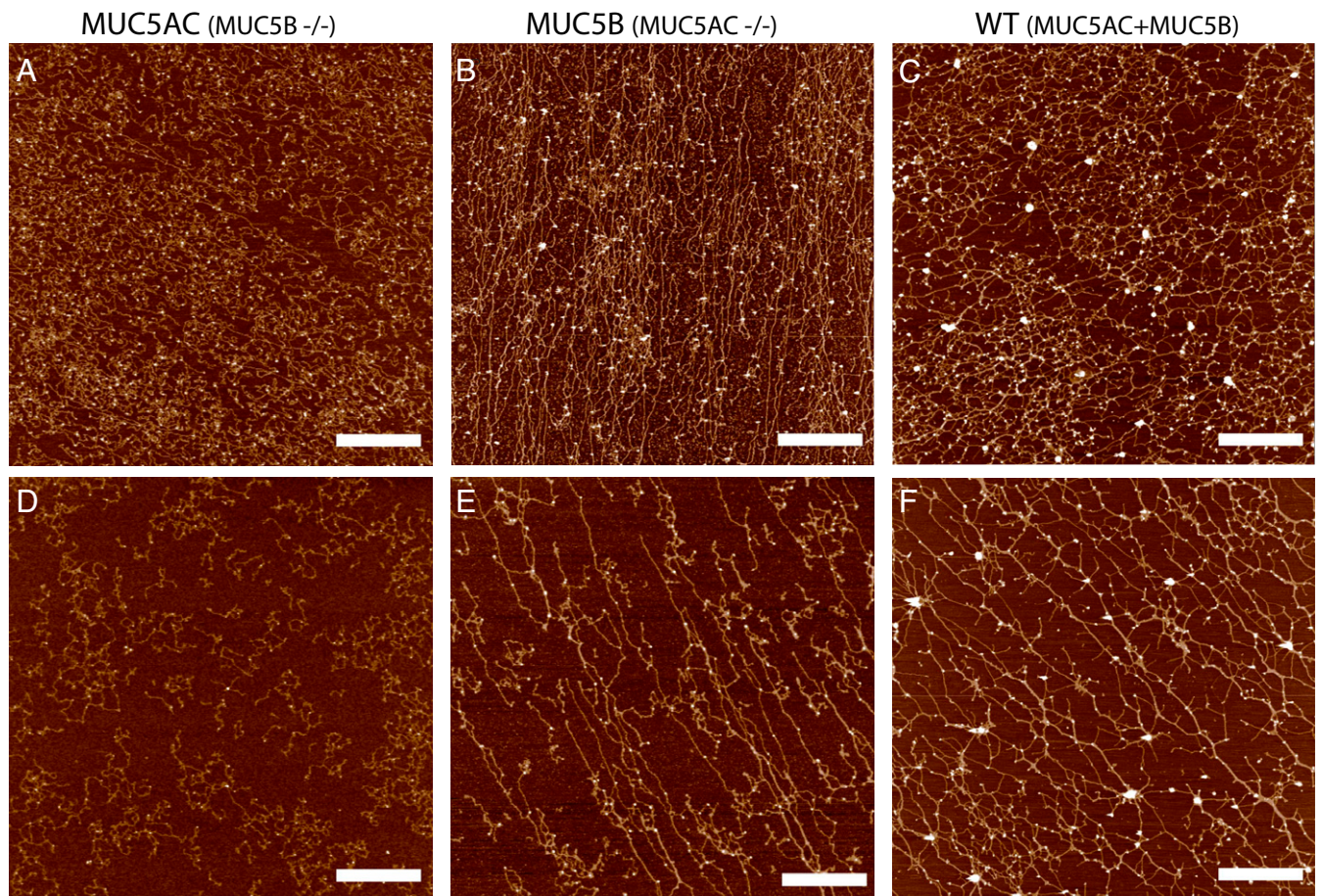


Fig. 2. Isolated MUC5AC and MUC5B from monomucin cultures exhibit distinct macromolecular organization on surfaces. AFM images of mucins MUC5AC (A), MUC5B (B), and WT secretions (C) at a high concentration (~100 µg/mL) and also imaged at a lower concentration ~30 µg/mL (D–F). MUC5AC mucin polymers (A, D) form more compact structures with fewer (if any) long linear structures, while MUC5B (B, E) networks form polymers with a higher frequency of linear straight structures. WT Calu3 secretions (C, F), which contain both MUC5AC and MUC5B mucins at a 3:1 ratio exhibit a distinct mucin network that combines elements of both monomucin networks. (Scale bar, 1 µm.)

Putative Leucine-Rich Zipper Region Plays an Essential Role in Structural Stability. To elucidate the role of the putative MUC5AC-specific LZ region toward the carboxyl-terminal end of the D1 domain on the molecular organization and integrity of the N-terminal region of MUC5AC, a construct was generated and expressed that replaced the four leucine residues in the LZ region with alanine. This mutated N-terminal construct of MUC5AC with the altered LZ region (5ACNT-LZ) was isolated from ~5 L conditioned 293-EBNA medium using a nickel affinity column followed by a combination of SEC and anion exchange chromatography. The final products were analyzed by SDS-PAGE in both native and reduced states and by SEC-MALLS (Fig. 6).

The SDS-PAGE gels indicated that the 5ACNT-LZ expression profile differed from the native 5ACNT, exhibiting multiple distinct bands between ~55 kDa and ~500 kDa with no evidence of the 5ACNT monomer, dimer, and trimer bands. Western blot and mass spectrometry peptide coverage analysis after in-gel digestion of the SDS-PAGE bands indicated that the 5ACNT-LZ product was missing the D3 domain (SI Appendix, Fig. S5). The molecular masses from the SDS-PAGE of the unreduced 5ACNT-LZ expressed proteins indicated dimers and trimers of the D1-D2 (theoretical MW 71,561 kDa) and D1-D2-TIL (theoretical MW 96,724 kDa) at around 144, 194, 216, and 271 kDa. This was consistent with data obtained by SEC-MALLS (Fig. 6C). After reduction, SDS-PAGE analyses indicated three dominant protein bands around 61, 72, and 100 kDa (Fig. 6A). Mass spectrometry

analysis of the bands displayed on the SDS-PAGE confirmed that the 68-kDa band in the unreduced sample band is missing a part of the D' and the entire D3 domain. The bands, 87 and 127 kDa, were also missing the D3 domain (SI Appendix, Fig. S5).

Discussion

The biologic advantage of having two secreted mucins with similar domain structures in the airways remains a mystery. Other than MUC5AC containing two additional Cys-D domains in the central glycosylated regions and a unique putative LZ motif in the N-terminal region, the architecture of the protein backbones of the two secreted mucins is rather comparable. Available evidence suggests that MUC5B is necessary for lung homeostasis and defense (4, 7), while MUC5AC is expressed in response to stress and often becomes a hallmark of disease activity (4, 8, 10, 11). How these functional differences in MUC5AC and MUC5B are coupled to their structural features, macromolecular assembly, and mucus gel infrastructures is not well understood.

Our AFM data demonstrate a distinct difference between the macromolecular structures of isolated MUC5B and MUC5AC; MUC5B was dominated by long linear strands, whereas MUC5AC multimers exhibited a higher degree of branching and formed more compact structures. The fact that our SEM observations of the mucins on cell culture demonstrate similar morphology is strong evidence that these are inherent properties of the mucins and not merely an artifact of either imaging modality. Interestingly, WT

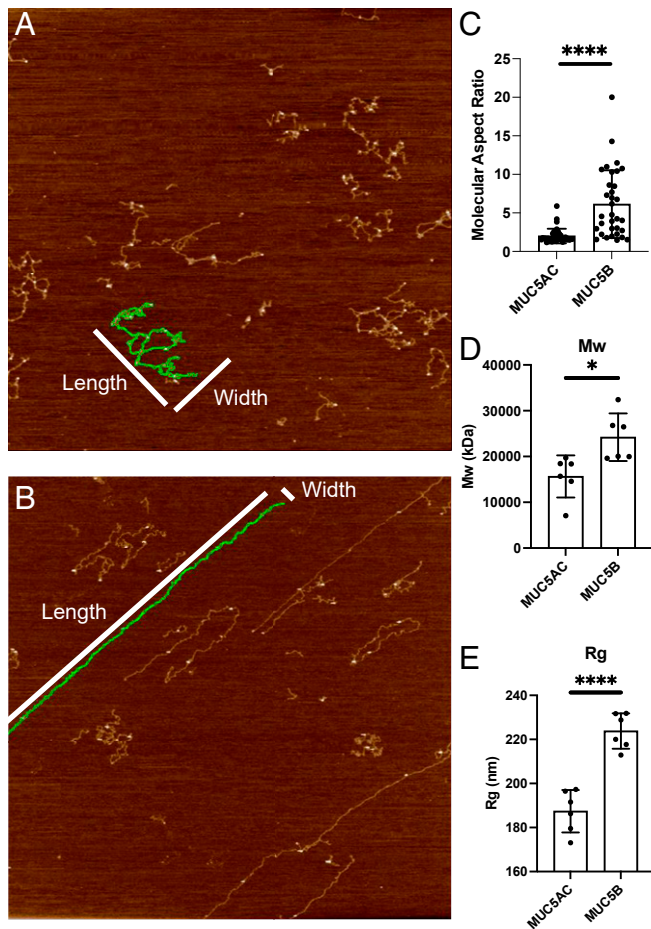


Fig. 3. Distinct macromolecular properties of MUC5AC and MUC5B mucins on surfaces: Aspect ratio analysis was performed on images of dilute MUC5AC (A) and MUC5B (B) preparations using AR16.10.211 software (Oxford Instruments). Selected images had less than 4% mucin coverage to enable the analysis of isolated macromolecules. Images were first flattened (Flatten 0) and then segmented by masking the image at 350 picometers, dilating the mask, and then running the analyze particles job to segment particles excluding particles with diameters less than 50 nm. The aspect ratio (length/width, with length being the longer dimension) of particles was recorded across several images for both the MUC5AC sample and the MUC5B sample. (C) MUC5AC macromolecules have a low aspect ratio, while MUC5B macromolecules have both high (dominant) and sometimes low aspect ratio macromolecules. SEC-MALLS analysis shows that MUC5B has both a higher average (D) MW and (E) radius of gyration. * $P = 0.05$, **** $P < 0.0001$.

CALU3 secretions containing both MUC5AC and MUC5B, imaged with SEM in situ on the apical surface of the cells and on a mica surface for AFM, exhibited combined features (long filaments and branched structures) seen in the individual monomucin preparations. We observed similar results when we mixed isolated MUC5AC and MUC5B preparations together (*SI Appendix, Fig. S1*). These findings suggest that the two polymeric mucins interact and interpenetrate with each other either directly or via interacting proteins to make a net-like gel structure and that both MUC5B and MUC5AC are important elements for the formation of an effective airway mucus barrier framework. This differs from previous studies that utilized immunofluorescence microscopy and observed that the two mucins were distinctly localized without mixing in IL-13-treated airway cell cultures (23, 28) and severe asthmatic sputum samples (23). One possible explanation of these different observations could be ascribed to the techniques used. Immunofluorescent microscopy is highly dependent on

antibody mobility, signal intensity, and epitope access; a tighter mucin network might sterically hinder antibodies and restrict their mobility/epitope access. Another potential explanation could be in the experimental conditions; our data were of mucins/mucus from a “normal” condition in which mucins and other related proteins are secreted at a basal rate and baseline concentrations, while the prior studies imaged severe asthmatic sputum (23) and IL-13 stimulated human tracheobronchial epithelial cell cultures (23, 28) with highly elevated mucin/mucus concentrations.

We further investigated the biophysical differences in the mucins by quantifying the biophysical properties of the layers that they formed on a hydrophobic surface via QCM-D. We found that in a concentration-controlled experiment, more MUC5AC deposited onto the surface than MUC5B, which suggests that MUC5AC may be “stickier” than MUC5B. Further analysis showed that MUC5AC formed a denser, stiffer, and more viscoelastic layer than MUC5B. These biophysical measurements, along with our imaging data, indicate a structural and functional difference between MUC5AC and MUC5B networks.

As these mucins demonstrate similar domain structures, we hypothesized that the distinct structural networks formed by the MUC5AC and MUC5B were due to differences in multimerization of the N-terminal regions of the two mucins. There are reports indicating that the N-terminal multimerization process might be mucin specific. There is a consensus that MUC5B exclusively forms dimers through its N-terminal region, while MUC2’s N-terminal multimerization seems less agreed upon; it has been reported that MUC2 forms trimers (18) or dimers (19). How MUC5AC multimerizes through its N-terminal region and how this effects the differences observed in the imaging and QCM-D results remains an open question.

To understand if the distinct topographic and viscoelastic features of MUC5AC gels are coupled to its (macro-)molecular assembly, we created a MUC5AC N-terminal construct (5ACNT) consisting of the D1-D2-D’-D3 domains. Utilizing the recombinant protein product 5ACNT, we characterized the (macro-)molecular organization of the whole N-terminal region of MUC5AC. This approach allowed us to elucidate differences between MUC5AC and other secreted mucin N-terminal structures and how these differences may influence the properties of MUC5AC hydrogels. Important observations were evident from our findings. First, the recombinant 5ACNT protein and the N-terminal regions of native MUC5AC were found to assemble into both dimers and higher-order multimers including trimers and tetramers as observed by SDS-PAGE, SEC-MALLS, and StcE digestion of the native MUC5AC. Second, there was no apparent pH-dependent, Ca^{2+} -mediated, noncovalent multimeric assembly observed with 5ACNT.

The SDS-PAGE and SEC-MALLS analyses indicated that the 5ACNT formed as dimers (40%), trimers (30%), and, to a lesser extent, monomers (20%) and tetramers (10%). This finding was further validated by the StcE digestion of native MUC5AC, which agreed with the results seen with expressed N-terminal protein. Specifically, digestion of the central glycosylated region of MUC5AC generated N-terminal fragments, which were organized mostly as dimers and trimers. Using high concentrations of SDS and urea in the SDS-PAGE sample buffer did not affect the presence of dimers, trimers, and tetramers. However, upon DTT reduction, these bands collapsed into a single band representing the monomer, suggesting disulfide bonding-mediated multimer assembly.

There are limited data on the N-terminal oligomerization sites of MUC5AC. With regard to dimerization versus trimerization as a structure for MUC5AC, we can speculate based on previous findings of the similar N-terminal multimerization domains of porcine submaxillary mucins and MUC2 (29, 30). The *CGLCG* motif in the D1 and D3 domains of porcine submaxillary mucin are important for N-terminal folding at low pH and for N-terminal multimerization via the *GLCSWR* motif in the D3 domain.

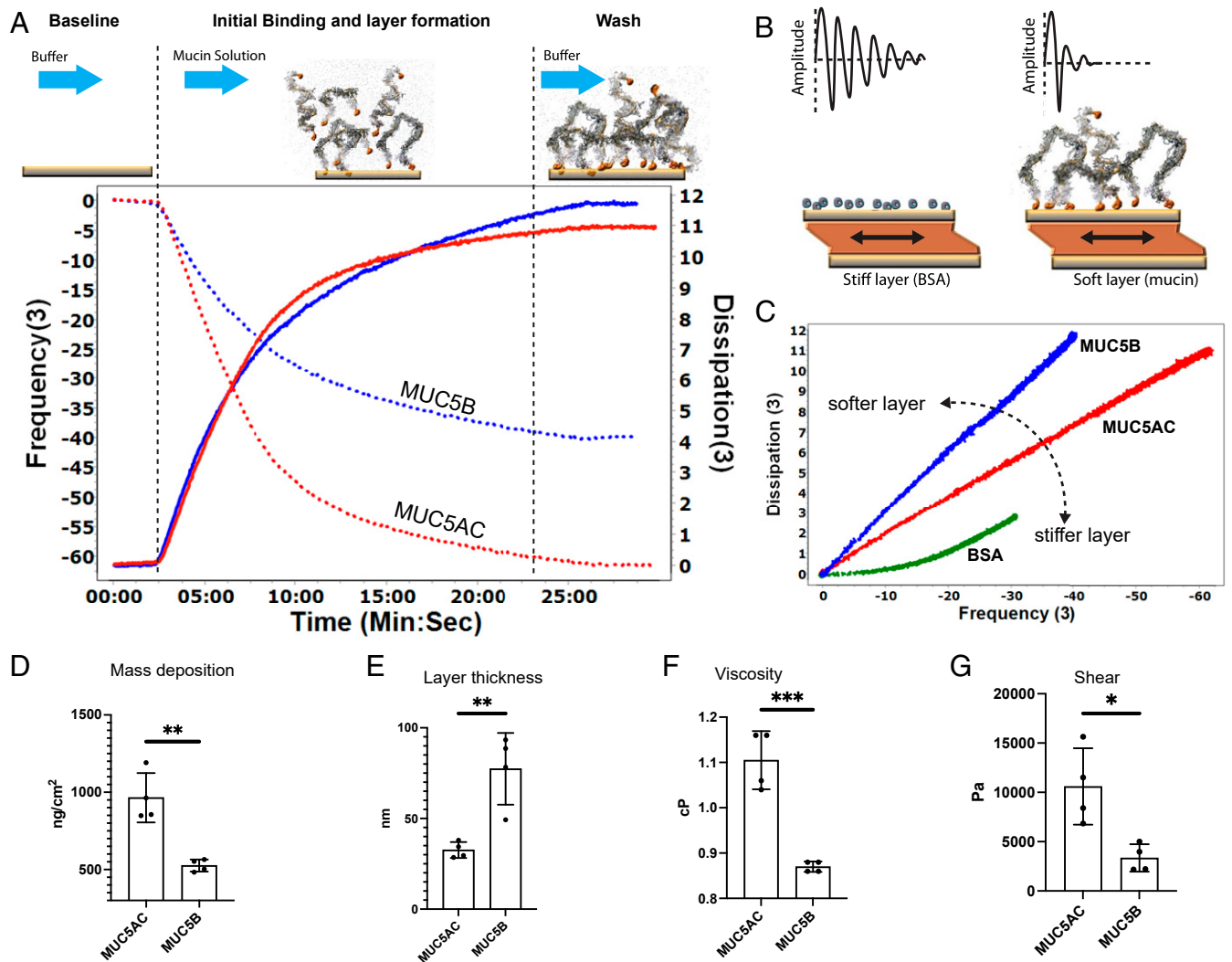


Fig. 4. QCM-D experiments indicate that MUC5AC forms stiffer, denser, and more viscoelastic layers compared to MUC5B. (A) A cartoon depicting the time course of a QCM-D experiment with representative data for measurements with MUC5AC and MUC5B shown underneath. At the same concentration (100 $\mu\text{g}/\text{mL}$), the frequency shift of the F3 overtones (dotted lines) and the dissipation shift for D3 (solid lines) were monitored while MUC5AC (red) and MUC5B (blue) were being deposited in the gold QCM-D chip. (B) The cartoon shows that for a material that is tightly coupled to the crystal (e.g. bovine serum albumin, BSA) there is a gradual decay in the amplitude. For a “softer” layer that has more interaction with the buffer (such as mucin), the damping occurs much faster. (C) A typical plot for dissipation versus frequency shifts ($\Delta\text{D}/\Delta\text{F}$) during the absorption of MUC5AC (red) and MUC5B (blue). MUC5AC forms a stiffer, denser layer. The slope of a BSA layer, which forms a solid and nondissipating layer, is shown for comparison (green). (D) The Sauerbrey model calculated an absorbed MUC5AC layer of $964 \pm \text{SD } 159 \text{ ng} \cdot \text{cm}^{-2}$ and MUC5B layer of $526 \pm \text{SD } 39 \text{ ng} \cdot \text{cm}^{-2}$, $n = 4$. (E–G) Voight modeling determined that (E) the MUC5AC layer was much thinner/denser ($32.6 \text{ nm} \pm \text{SD } 4.4$, $n = 4$) compared to the MUC5B layer ($77.4 \text{ nm} \pm \text{SD } 19.7$, $n = 4$, $P = 0.0045$) and that (F) the relative viscosity ($1.105 \text{ cP} \pm \text{SD } 0.06$, $n = 4$) and (G) shear elasticity ($10,600 \text{ Pascal} \pm \text{SD } 3,800$, $n = 4$) of MUC5AC layers were significantly higher compared to the relative viscosity ($0.87 \text{ cP} \pm \text{SD } 0.01$, $n = 4$) and shear elasticity ($3,300 \text{ P} \pm \text{SD } 1,400$, $n = 4$) ($P = 0.02$) of the MUC5B layer. $*P \leq 0.05$, $**P \leq 0.01$, $***P \leq 0.005$ (a more detailed legend can be found in *SI Appendix, Fig. S6*).

5ACNT also has the *CGLCG* motif within all three D domains (D1, D2, and D3). Also, it has recently been shown that MUC2 dimerizes through disulfide bonds at $C^{1088}\text{ECFC}$ and $C^{1130}\text{EWH}$ that correspond to $C^{1137}\text{ECFC}$ and $C^{1174}\text{EWH}$ in the D3 domain of MUC5AC (19, 29). As highlighted in these studies, the likely site for 5ACNT dimerization is via one of the putative dimerization sites in the D3 domain; $C^{1137}\text{ECFC}$ or $\text{PEGQC}^{1174}\text{EWH}$. However, the dimerization and higher-order multimerization site(s) of the N-terminal region of MUC5AC remain to be determined by future structural studies.

These observations reported here suggest that the N-terminal region of MUC5AC assembles differently than that of MUC5B, which assembles only as dimers through its N-terminal region (17). The MUC5B organization results in a linear macromolecular structure that forms a transportable gel that is essential for

mucociliary clearance (7). This organization may explain why MUC5B is the dominant mucin in airway mucociliary homeostasis. The unique feature of MUC5AC described here (i.e., the ability to both dimerize and trimerize/tetramerize via its N-terminal region) gives MUC5AC the ability to make a tighter gel, which protects the epithelium from pathological and chemical insults. The stomach environment is a prime example of this requirement. The MUC5AC-dominated mucus gel layer in the stomach protects the epithelium from the harsh, highly acidic gastric luminal environment. Although the role of MUC5AC in the lung still not clear, we speculate that it may serve a similar role as it does in the stomach. In the lung, MUC5AC protects against invasive pathogens, including viruses, and prevents parasite migration through the lung.

MUC5AC is not essential for mucociliary clearance (7), and it is expressed in response to stress in the lung, notably present as

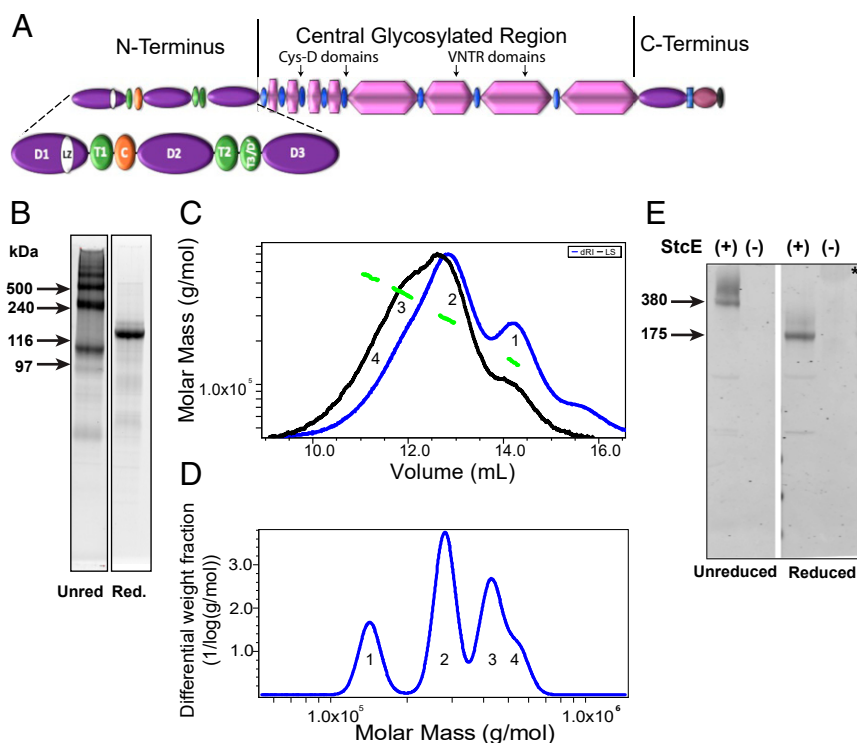


Fig. 5. 5ACNT forms dimers, trimers, and higher-order oligomers: (A) Cartoon showing the 5ACNT construct in relation to the entire molecule. The construct contains the D1, D2, D', and D3 domains of the N-terminal region. (B) SYPRO Ruby staining of SDS-PAGE of purified protein shows that the unreduced (Unred) 5ACNT construct produced monomers, dimers, trimers, and higher-order oligomers. A second gel shows that upon reduction (Red.), these all collapse into a single band. (C) This panel shows traces of the purified 5ACNT protein on a Superose 6 column monitored by the tREX refractometer (blue) and Heleos II multiangle laser light scattering (black). The molar masses, as obtained from the MALLS, are plotted across the 5ACNT distribution (green). (D) Molar mass distribution of MUC5AC N-terminal multimers (1 = monomer, 2 = dimer, 3 = trimer, and 4 = tetramer). (E) A Western blot stained with MUC5AC antibodies against the D2 and D3 domains reveals that enzymatically treating whole-length MUC5AC with StcE, which cleaves the molecule within the O-linked glycosylation region, thus leaving the terminals intact, shows that the native MUC5AC N-terminal domains are organized into dimers, trimers, and higher-order oligomers. These bands collapse upon reduction. * = Untreated, reduced native MUC5AC (MW around 2.5 MDa) hardly enters the gel. VNTR, Variable number of tandem repeats.

part of the pathogenesis of chronic lung conditions such as cigarette smoke-driven CB and COPD (4) and Th2-driven asthma (9, 23). Unlike the stomach and colon, the functional requirement for lung health is a nonadhesive, mobile mucus layer that can be easily transported by the ciliary escalator. This objective is mainly achieved by the dominant MUC5B mucin that makes a gel based on linear polymers in optimum conditions. In the stressed lung, in response to cigarette smoke and other inflammatory conditions, however, MUC5AC concentration and the MUC5AC/MUC5B ratio increases (4). Increased MUC5AC concentrations, up to 10-fold, are closely related to pathologies in the airways, including declined lung function and small airway abnormalities (8). In Th2 high allergic asthma, MUC5AC increases more dramatically, up to 10- to 50-fold, and becomes the dominant airway mucin. Collectively, raised MUC5AC levels in the airways are closely associated with airway obstruction in CB, COPD, asthma, and other muco-obstructive lung diseases. We speculate that the tight gel formed by MUC5AC is beneficial in isolating acute insults, including viruses that are known to induce type I inflammation (20) and parasites that are known to induce type II inflammation (11) but proves pathological in chronic conditions.

In addition to the organization of the mucus gel, N-terminal organization of gel-forming mucins is critical with respect to how large molecules are assembled and efficiently stored inside 0.5- to 1- μm intracellular mucin granules. Gel-forming mucins are compactly stored in the secretory granules under low pH and high Ca^{2+} . There are Ca^{2+} binding sites in the N-terminal region of mucins that apparently play an important role in mucin polymer intragranular

organization. MUC5B, for instance, forms noncovalent, reversible calcium-mediated cross-links at pH 6 at the N-terminal D3 domain (17) and forms head-to-head tetramers (31). MUC2 mucin has been reported to form an N-terminal Ca^{2+} -mediated pH-dependent supramolecular organization that requires CysD domains that have calcium binding motifs (32). To investigate whether the 5ACNT utilizes Ca^{2+} and pH-dependent associations for cross-linking/multimerization, we incubated 5ACNT with calcium and low pH. Notably, we did not observe increased multimerization in response to these treatments. This finding suggests that the 5ACNT protein may not have a calcium binding site. As MUC2 is reported to require CysD domains to form a Ca^{2+} and pH-dependent supramolecular organization (32) and the 5ACNT construct does not contain a CysD domain, we can surmise that 5ACNT does not express the Ca^{2+} binding sites to form noncovalently cross-linked multimeric structures and may require a CysD like MUC2.

Unlike other mammalian gel-forming mucins, MUC5AC has a putative LZ region toward the carboxyl-terminal end of its D1 domain. The function of this unique domain on the molecular organization of the monomer and multimer formation has not been experimentally investigated. It has been proposed that it facilitates a helix formation within the region to allow noncovalent intermolecular interactions for multimerization (16). To understand the function of this domain, we mutated the four leucine residues within the putative LZ region to alanine. The SDS-PAGE and SEC-MALLS analyses indicated that the product from this construct was strikingly different from the nonmutated WT protein. Firstly, the purified

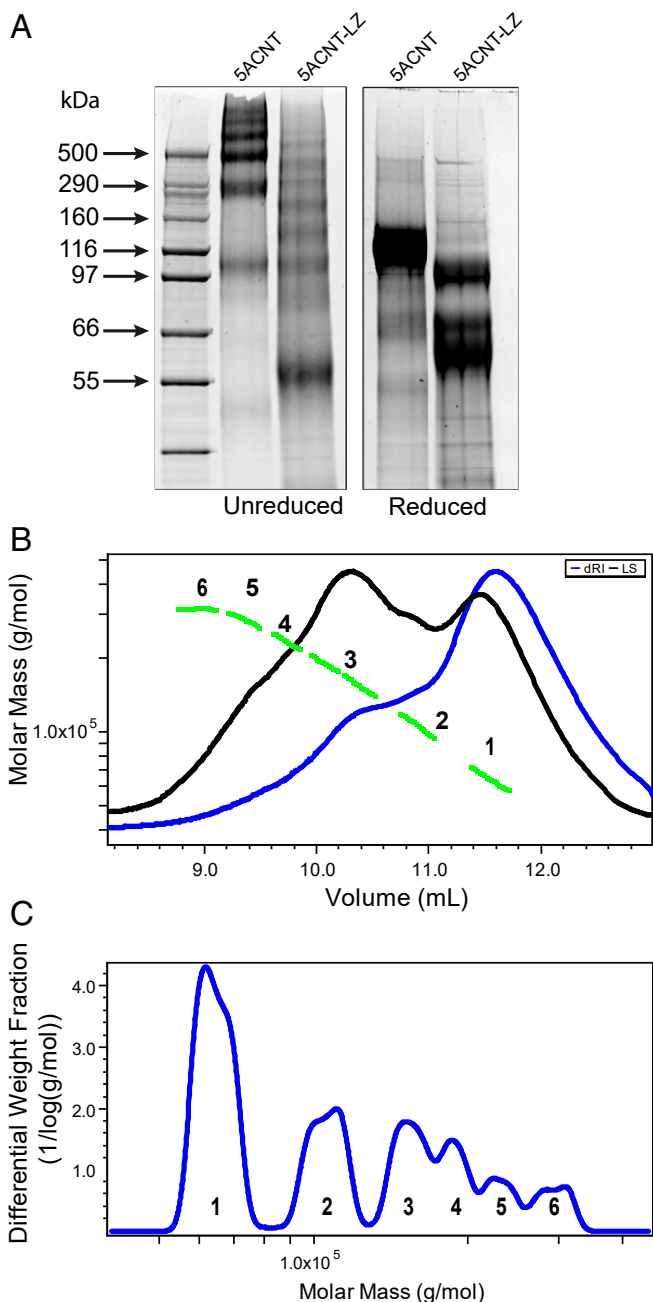


Fig. 6. MUC5AC N-terminal domain with a mutated LZ (5ACNT-LZ) displays a different multimerization profile: (A) SYPRO Ruby staining of SDS-PAGE of purified protein products shows that 5ACNT-LZ maintains the ability to form higher-order oligomers, bands ranging from 55 to 500 kDa, despite no longer having the D3 domain present. For mass spectrometry analyses of the bands, see *SI Appendix, Fig. S5*. When reduced, the 5ACNT-LZ shows three monomeric bands, as compared to 5ACNT, which produced only one band after reduction. (B) SEC-MALLS analysis of the 5ACNT-LZ zipper-expressed protein shows traces of the purified 5ACNT-LZ protein on a Superose 6 column monitored by the tREX refractometer (blue) and Helelos II multiangle laser light scattering (black). The molar masses, obtained from MALLS, are shown across the 5ACNT-LZ distribution (green). (C) Molar mass distribution of 5ACNT-LZ multimers. Increasing molecular weight peaks are represented with numbers (1 to 6).

5ACNT-LZ product did not contain a D3 domain. Second, the 5ACNT-LZ product still formed multimers of the D1-D2-D' domains. This observation suggests that the LZ domain may play

an important role in the stability of the whole N-terminal region of MUC5AC, likely providing a helical turn that precisely orients the molecule to form intramolecular disulfide bond formations between multiple cysteines of the remaining D domains. There is limited information on the N-terminal organization and the potential oligomerization sites of the MUC5AC gel-forming mucin. The *CGLCG* motif in the D1, D2, and D3 domains of MUC5AC is important for proper folding of the N terminus at low pH and also for multimerization via the *GLCSWR* motif in D3 (29, 30). The *CGLCG* motif in the D1 domain can also be involved in trans-Golgi multimerization (29). Given the fact that 5ACNT-LZ is missing the D3 domain, we can surmise that the multimers of 5ACNT-LZ were formed via the *CGLCG* in the D1 and/or D2 domains. Further investigations will be required to understand the fate of the D3 domain and the role of putative LZ domain in assembly, structure, and function of MUC5AC.

In conclusion, our study provides insight into the macromolecular assembly of the N-terminal region of MUC5AC, suggesting that it is markedly different from MUC5B assembly. The distinct N-terminal organization of MUC5AC may explain the unique properties of branched/networked, more adhesive, stiffer, and viscous MUC5AC mucus gel and its contributions to stagnant and adherent/"tethered" mucus layers in disease. Collectively, our data suggest why MUC5AC is more closely associated the pathogenesis of chronic muco-obstructive lung diseases than MUC5B, which underpins the mucus gel that can be transported by cilia and maintain lung homeostasis.

Materials and Methods

Experiments on the CRISPR-Cas9–Manipulated and WT Airway Calu3 Cell Cultures and Their Secretions. Human airway Calu-3 cells with either MUC5B or MUC5AC CRISPR-Cas9 deleted (6), termed MUC5AC or MUC5B monomucin cultures, and WT Calu3 cultures, were grown on 12-well transwells and maintained at an air-liquid interface (ALI) for at least 3 wk. Cells were seeded at an initial density of 2.5×10^5 cells per insert and were initially fed apically and basally with a nonproprietary media termed "UNC-ALI." However, upon reaching 100% confluence, cultures were fed three times per week basolaterally with UNC-ALI media (33).

SEM Images of Calu3 MUC5AC and MUC5B Monomucin Cultures. To preserve the mucin network ultrastructure, unwashed Calu3 cultures grown at ALI were fixed with 2.5% glutaraldehyde in 0.1 M sodium cacodylate buffer overnight at 4 °C. Samples were washed with fixative-free buffer three times before dehydration in increasing concentrations of ethanol. Samples were then dried by carrying them through critical point drying in liquid CO₂ (Tousimis) and sputter coated with 8 nm gold-palladium alloy (Ted Pella). Images were acquired on a Zeiss Supra 25 field emission SEM (Zeiss) at 5 kV and a working distance of 5 mm. Imaging was performed at the University of North Carolina Microscopy Services Laboratory.

Isolation of Native MUC5AC and MUC5B Mucins. MUC5AC and MUC5B monomucin Calu3 cell cultures were washed once per week by apical administration of 100 μ L phosphate-buffered saline (PBS), incubation for 30 min, and then collection of the PBS along with harvested secretions. Culture secretions were pooled together and subjected to isopycnic density gradient centrifugation (initial density $\rho = 1.35$ g/mL) for mucin isolation (5, 34). Fractions were probed with MUC5AC and MUC5B antibodies (34). Mucin-containing fractions (around the density 1.35 to 1.40 g/mL) were pooled for further analyses.

AFM Imaging of Isolated Mucins. Isolated native MUC5AC and MUC5B were analyzed using AFM. The AFM substrate was prepared by pipetting 50 μ L 10 mM nickel chloride solution onto freshly cleaved mica followed by washing the surface with Milli-Q water. A total of 20 μ L mucin sample was then pipetted onto the surface and allowed to interact with the mica for 3 min. Unbound material was removed by pipetting Milli-Q water onto and off of the mica. The sample was dried using a nitrogen gun and imaged using a Cypher AFM (Asylum/Oxford Instruments). Imaging was performed using Arrow UHFAUD tips (Nanoworld) using noncontact AM/FM tapping mode. AFM analysis of aspect ratio is described in Fig. 3.

QCM-D Measurements of Individual Mucins. MUC5AC- and MUC5B-surface interactions and the structural properties of the adsorbed MUC5AC and MUC5B layers were measured by QCM-D (Q-Sense, Biolin Scientific) using gold-coated chips. As a micromechanical method, QCM-D dynamically measures the amount and the density of the bound mass and the biophysical properties such as viscosity/elasticity and rigidity/hydration of the layers of (macro-)molecules. We have successfully applied this unique method in the past to measure the functions of mucins and their interactions with other proteins (35, 36). The concentrations of MUC5AC and MUC5B standards, which were isolated from pooled Calu3 secretions, were measured by SEC-MALLS-dRI and adjusted to ~100 $\mu\text{g}/\text{mL}$ in a 200-mM NaCl solution with 10 mM EDTA before being utilized for QCM-D. MUC5AC and MUC5B were deposited on a gold-coated QCM-D chip until a saturation level was achieved (~20 to 30 min). All experiments were conducted at a constant temperature of 23 °C. The solutions were applied over the gold-coated crystal at 30 $\mu\text{L}/\text{min}$. The changes in the frequency (mucin deposition) and dissipation (mucin layer rigidity and hydration) of the crystal were measured at its resonance frequency at its fundamental frequency and overtones (15, 25, 35, 45, 55, and 65 MHz). Further analysis of the mucin layers was performed using Q-tools software (Biolin Scientific). The quantity of the bound molecules was calculated utilizing the Sauerbrey model (25). The viscoelasticity and thickness of the mucin layers were calculated by applying the Voigt viscoelastic model. In brief, the Voigt model treats the viscoelastic material (in our case, the mucin layer) as a spring and dashpot in parallel. Considering the frequency and dissipation changes across multiple overtones and knowing the displacement of the sensor, fluid density, and viscosity makes it possible to model the viscosity and elasticity of the layer (26).

Expression and Purification of Native and Mutated MUC5AC N-Terminal Proteins. The human MUC5AC N-terminal sequence (AJ298317.1, 120~3692 bp, protein sequence CAC83674.1, amino acids 28~1218) was inserted between the XhoI and BamHI sites of the mammalian episomal expression vector pCEP-His (17). To investigate the role of the potential LZ domains in the D1 domain of the N-terminal region, a 5ACNT-LZ mutant was constructed that changed the leucine residues at positions 274, 281, 288, and 295 to alanine. The resulting plasmids for 5ACNT and 5ACNT-LZ were pCEP-His-MUC5ACNT and pCEP-His-MUC5ACNT-LZ, respectively. The 293-EBNA cells were cultured in Dulbecco's Modified Eagle Medium (DMEM) with 10% fetal bovine serum (FBS). pCEP-His-MUC5ACNT or pCEP-His-MUC5ACNT-LZ was transfected into 293-EBNA cells using Lipofectamine 2000 (Invitrogen), and cells were selected by treating with 1 $\mu\text{g}/\text{mL}$ puromycin for at least 7 d. Stably transfected 293-EBNA cells were cultured in DMEM with 10% FBS and 0.5 $\mu\text{g}/\text{mL}$ puromycin until confluence. The medium was then changed to DMEM/F12 with GlutaMax (Gibco) and 0.05% Protease Inhibitor Mixture (Sigma-Aldrich). Conditioned medium was collected every 3 or 4 d for 2 to 3 wk and dialyzed against Tris-Imidazole buffer (20 mM Tris base, 0.4 M NaCl, and 10 mM Imidazole, pH 7.4) before protein purification. His-MUC5ACNT and His-MUC5ACNT-LZ recombinant proteins were sequentially purified with a GE HisTrap Fast Flow 1-mL column (eluted in Tris-Imidazole buffer with 100 mM imidazole), a Superose 6 size-exclusion column (eluted in 25 mM Tris, 10 mM NaCl, pH 7.4), and a Resource Q anion exchange column (eluted with a gradient of 0~0.5 M NaCl in 25 mM Tris, pH 7.4).

SEC-MALLS Characterization of Purified MUC5ACNT and MUC5ACNT-LZ. To characterize protein macromolecular properties, 5ACNT and 5ACNT-LZ proteins after purification were applied to a WTC-050N5 size-exclusion column (Wyatt, 5 μm , 500 Å, 4.6 mm \times 300 mm) in 25 mM Hepes and 150 mM NaCl and eluted at 0.5 mL/min. Column eluents were passed through an inline HELEOSII MALLS with a quasi-elastic dynamic light-scattering attachment and an Opti-lab TrEX refractometer. To investigate the effects of Ca^{2+} and pH on protein stability and organization, aliquots of 5ACNT protein were dialyzed and incubated overnight at 4 °C either in 10 mM CaCl_2 pH 7.4, 10 mM CaCl_2 pH 6.0, or 5 mM ethylene glycol-bis(β -aminoethyl ether)-N,N,N',N'-tetraacetic

acid (EGTA) at pH 7.4 or pH 6 and then applied to a WTC-050N5 4.6/300 column in 25 mM Hepes, 150 mM NaCl (with CaCl_2 or EGTA at pH 7.4 or pH 6 at room temperature). Data were analyzed using ASTRA software (version 7.0).

SYPRO Ruby Protein Gel Staining and Western Blot Staining. Purified 5ACNT and 5ACNT-LZ proteins were analyzed with SDS-PAGE and SYPRO Ruby staining (Molecular Probes) following the manufacturer's instructions. Proteins were visualized using a 300-nm ultraviolet transilluminator, and bands of interest were sliced out and collected for in-gel digestion as previously described (37). Western blots were probed with polyclonal antibodies 5ACD2 (against the MUC5AC D2 domain), and 5ACD3 (against the MUC5AC D3 domain), which were raised in rabbits against the peptide sequences CGFNFSIQADDFR and CFDDIAVNDFAFR, respectively.

Proteomic Analysis by Liquid Chromatography Tandem Mass Spectrometry. Isolated 5ACNT and 5ACNT-LZ proteins were subjected to liquid chromatography tandem mass spectrometry (LC-MS/MS)-based proteomic analysis after in-solution or in-gel digestion. In-solution-digested samples were prepared for mass spectrometry analysis utilizing filter-aided sample preparation (38), as described previously (39). In-gel digestion of selected SYPRO Ruby-stained SDS-PAGE bands was performed as previously described (37). The resulting peptides from both digestion methods were injected for mass spectrometry analyses into a Q Exactive (Thermo Fisher Scientific) mass spectrometer coupled to an UltiMate 3000 (Thermo Fisher Scientific) nano high-performance liquid chromatography (HPLC) system, as described previously (40). The acquired raw data were processed using the Proteome Discoverer 1.4 (Thermo Fisher Scientific) software and searched against the UniProt protein database (Homo sapiens, April 2019) or the MUC5ACNT construct sequence using the MASCOT search engine with the following parameters: 10 ppm mass accuracy for parent ions, 0.02 Da accuracy for fragment ions, and two missed cleavages allowed. Carbamidomethyl modification of cysteine was specified as a fixed modification, and oxidation of methionine was specified as a variable modification. Scaffold 4.7.5 (Proteome Software Inc.) was used to validate MS/MS-based peptide and protein identifications. Peptide identifications were accepted if they could be established at greater than 99.0% probability by the Scaffold Local False Discovery Rate algorithm. Peptide quantification was performed using total ion chromatogram intensities.

StcE Digestion of Isolated Native MUC5AC. MUC5AC, derived from Calu3 cells and A549 cells, was dialyzed overnight against PBS using Slide-a-Lyzers (Pierce) with a 3-kDa MW cutoff. MUC5AC from each cell line was separated into two identical aliquots and then treated with 1.5 μL StcE (1.5 μg) or the equivalent volume of PBS, which served as a control. The samples were then incubated at 37 °C for 1 h. After incubation, the samples were prepared for SDS-PAGE by the addition of running buffer. Each sample was split so that it could be run both reduced and unreduced.

Statistical Analysis. Where applicable, the statistical analyses were performed using the unpaired samples Student's *t* test.

Data Availability. All study data are included in the article and/or *SI Appendix*.

ACKNOWLEDGMENTS. This work was supported by grants from the NIH; R01HL103940, R01HL110906, and 5U01HL137880; from the COPD Foundation; from the Cystic Fibrosis Foundation, SUBRAM1710; and from the Medical Research Council (MR/R002800/1). The Wellcome Trust Centre for Cell-Matrix Research, University of Manchester, is supported by core funding from the Wellcome Trust (Grant No. 088785/Z/09/Z). We thank Dr. Brian Button for providing the recombinant StcE and Dr. Richard Boucher for critically reading the manuscript.

- M. E. Johansson *et al.*, The inner of the two Muc2 mucin-dependent mucus layers in colon is devoid of bacteria. *Proc. Natl. Acad. Sci. U.S.A.* **105**, 15064–15069 (2008).
- H. Nordman *et al.*, Gastric MUC5AC and MUC6 are large oligomeric mucins that differ in size, glycosylation and tissue distribution. *Biochem. J.* **364**, 191–200 (2002).
- E. C. Veerman *et al.*, Distinct localization of MUC5B glycoforms in the human salivary glands. *Glycobiology* **13**, 363–366 (2003).
- M. Kesimer *et al.*, Airway mucin concentration as a marker of chronic bronchitis. *N. Engl. J. Med.* **377**, 911–922 (2017).
- M. Kesimer *et al.*, Tracheobronchial air-liquid interface cell culture: A model for innate mucosal defense of the upper airways? *Am. J. Physiol. Lung Cell. Mol. Physiol.* **296**, L92–L100 (2009).
- K. Okuda *et al.*, Localization of secretory mucins MUC5AC and MUC5B in normal/healthy human airways. *Am. J. Respir. Crit. Care Med.* **199**, 715–727 (2019).
- M. G. Roy *et al.*, Muc5b is required for airway defence. *Nature* **505**, 412–416 (2014).
- G. Radicioni *et al.*, Airway mucin MUC5AC and MUC5B concentrations and the initiation and progression of chronic obstructive pulmonary disease: An analysis of the SPIROMICS cohort. *Lancet Respir. Med.*, 10.1016/S2213-2600(21)00079-5 (2021).
- J. L. Cho *et al.*, Allergic asthma is distinguished by sensitivity of allergen-specific CD4+ T cells and airway structural cells to type 2 inflammation. *Sci. Transl. Med.* **8**, 359a132 (2016).
- C. M. Evans *et al.*, The polymeric mucin Muc5ac is required for allergic airway hyperreactivity. *Nat. Commun.* **6**, 6281 (2015).

11. S. Z. Hasnain *et al.*, Muc5ac: A critical component mediating the rejection of enteric nematodes. *J. Exp. Med.* **208**, 893–900 (2011).
12. M. P. Buisine *et al.*, Genomic organization of the 3'-region of the human MUC5AC mucin gene: Additional evidence for a common ancestral gene for the 11p15.5 mucin gene family. *Biochem. J.* **332**, 729–738 (1998).
13. J. L. Desseyn, M. P. Buisine, N. Porchet, J. P. Aubert, A. Laine, Genomic organization of the human mucin gene MUC5B. cDNA and genomic sequences upstream of the large central exon. *J. Biol. Chem.* **273**, 30157–30164 (1998).
14. R. Cao, T. T. Wang, G. DeMaria, J. K. Sheehan, M. Kesimer, Mapping the protein domain structures of the respiratory mucins: A mucin proteome coverage study. *J. Proteome Res.* **11**, 4013–4023 (2012).
15. D. J. Thornton, K. Rousseau, M. A. McGuckin, Structure and function of the polymeric mucins in airways mucus. *Annu. Rev. Physiol.* **70**, 459–486 (2008).
16. J. H. van de Bovenkamp *et al.*, Molecular cloning of human gastric mucin MUC5AC reveals conserved cysteine-rich D-domains and a putative leucine zipper motif. *Biochem. Biophys. Res. Commun.* **245**, 853–859 (1998).
17. C. Ridley *et al.*, Assembly of the respiratory mucin MUC5B: A new model for a gel-forming mucin. *J. Biol. Chem.* **289**, 16409–16420 (2014).
18. D. Ambort *et al.*, Calcium and pH-dependent packing and release of the gel-forming MUC2 mucin. *Proc. Natl. Acad. Sci. U.S.A.* **109**, 5645–5650 (2012).
19. G. Javitt *et al.*, Intestinal gel-forming mucins polymerize by disulfide-mediated dimerization of D3 domains. *J. Mol. Biol.* **431**, 3740–3752 (2019).
20. C. A. Hewson *et al.*, Rhinovirus induces MUC5AC in a human infection model and in vitro via NF- κ B and EGFR pathways. *Eur. Respir. J.* **36**, 1425–1435 (2010).
21. D. Rajan *et al.*, MUC5AC levels associated with respiratory syncytial virus disease severity. *Clin. Infect. Dis.* **67**, 1441–1444 (2018).
22. E. Doz *et al.*, Cigarette smoke-induced pulmonary inflammation is TLR4/MyD88 and IL-1R1/MyD88 signaling dependent. *J. Immunol.* **180**, 1169–1178 (2008).
23. L. R. Bonser, L. Zlock, W. Finkbeiner, D. J. Erle, Epithelial tethering of MUC5AC-rich mucus impairs mucociliary transport in asthma. *J. Clin. Invest.* **126**, 2367–2371 (2016).
24. K. A. Ramsey *et al.*, Airway mucus hyperconcentration in non-cystic fibrosis bronchiectasis. *Am. J. Respir. Crit. Care Med.* **201**, 661–670 (2020).
25. G. Sauerbrey, Verwendung von Schwingquarzen zur Wägung dünner Schichten und zur Mikrowägung- Use of quartz crystal for weighing thin layers and microweighing. *Z. Phys.* **155**, 206–222 (1959).
26. M. V. Voinova, M. Rodahl, M. Jonson, B. Kasemo, Viscoelastic acoustic response of layered polymer films at fluid-solid interfaces: Continuum mechanics approach. *Phys. Scr.* **59**, 391–396 (1999).
27. S. A. Malaker *et al.*, The mucin-selective protease StcE enables molecular and functional analysis of human cancer-associated mucins. *Proc. Natl. Acad. Sci. U.S.A.* **116**, 7278–7287, 10.1073/pnas.1813020116 (2019).
28. B. D. Batson, "Airway mucin dynamics in infection and inflammation," PhD dissertation, University of North Carolina at Chapel Hill, NC, <https://doi.org/10.17615/148z-fg65> (2019).
29. J. Perez-Vilar, R. L. Hill, Identification of the half-cystine residues in porcine submaxillary mucin critical for multimerization through the D-domains. Roles of the CGLCG motif in the D1- and D3-domains. *J. Biol. Chem.* **273**, 34527–34534 (1998).
30. J. Perez-Vilar, A. E. Eckhardt, A. DeLuca, R. L. Hill, Porcine submaxillary mucin forms disulfide-linked multimers through its amino-terminal D-domains. *J. Biol. Chem.* **273**, 14442–14449 (1998).
31. S. Trillo-Muyo *et al.*, Granule-stored MUC5B mucins are packed by the non-covalent formation of N-terminal head-to-head tetramers. *J. Biol. Chem.* **293**, 5746–5754 (2018).
32. G. Javitt *et al.*, Assembly mechanism of mucin and von Willebrand factor polymers. *Cell* **183**, 717–729.e16 (2020).
33. M. L. Fulcher, S. Gabriel, K. A. Burns, J. R. Yankaskas, S. H. Randell, Well-differentiated human airway epithelial cell cultures. *Methods Mol. Med.* **107**, 183–206 (2005).
34. M. Kesimer *et al.*, Molecular organization of the mucins and glycocalyx underlying mucus transport over mucosal surfaces of the airways. *Mucosal Immunol.* **6**, 379–392 (2013).
35. M. Kesimer, J. K. Sheehan, Analyzing the functions of large glycoconjugates through the dissipative properties of their absorbed layers using the gel-forming mucin MUC5B as an example. *Glycobiology* **18**, 463–472 (2008).
36. G. Radicioni *et al.*, The innate immune properties of airway mucosal surfaces are regulated by dynamic interactions between mucins and interacting proteins: The mucin interactome. *Mucosal Immunol.* **9**, 1442–1454 (2016).
37. M. Kesimer, N. Kiliç, R. Mehrotra, D. J. Thornton, J. K. Sheehan, Identification of salivary mucin MUC7 binding proteins from *Streptococcus gordonii*. *BMC Microbiol.* **9**, 163 (2009).
38. J. R. Wiśniewski, A. Zougman, N. Nagaraj, M. Mann, Universal sample preparation method for proteome analysis. *Nat. Methods* **6**, 359–362 (2009).
39. S. H. Abdelwahab *et al.*, Cigarillos compromise the mucosal barrier and protein expression in airway epithelia. *Am. J. Respir. Cell Mol. Biol.* **63**, 767–779 (2020).
40. M. Kesimer *et al.*, Excess secretion of gel-forming mucins and associated innate defense proteins with defective mucin un-packaging underpin gallbladder mucocele formation in dogs. *PLoS One* **10**, e0138988 (2015).